Model of human immunodeficiency virus budding and self-assembly: Role of the cell membrane

Rui Zhang and Toan T. Nguyen
School of Physics, Georgia Institute of Technology, 837 State Street, Atlanta, Georgia 30332-0430, USA
(Received 30 March 2008; published 5 November 2008)

Budding from the plasma membrane of the host cell is an indispensable step in the life cycle of the human immunodeficiency virus (HIV), which belongs to a large family of enveloped RNA viruses, retroviruses. Unlike regular enveloped viruses, retrovirus budding happens *concurrently* with the self-assembly of the main retrovirus protein subunits (called Gag protein after the name of the genetic material that codes for this protein: Group-specific AntiGen) into spherical virus capsids on the cell membrane. Led by this unique budding and assembly mechanism, we study the free energy profile of retrovirus budding, taking into account the Gag-Gag attraction energy and the membrane elastic energy. We find that if the Gag-Gag attraction is strong, budding always proceeds to completion. During early stage of budding, the zenith angle of partial budded capsids, α, increases with time as $\alpha \propto t^{1/2}$. However, if the Gag-Gag attraction is weak, a metastable state of partial budding appears. The zenith angle of these partially spherical capsids is given by $\alpha_0 \simeq (\tau^2/\kappa\sigma)^{1/4}$ in a linear approximation, where κ and σ are the bending modulus and the surface tension of the membrane, and τ is a line tension of the capsid proportional to the strength of Gag-Gag attraction. Numerically, we find $\alpha_0 < 0.3\pi$ without any approximations. Using experimental parameters, we show that HIV budding and assembly always proceed to completion in normal biological conditions. On the other hand, by changing Gag-Gag interaction strength or membrane rigidity, it is relatively easy to tune it back and forth between complete budding and partial budding. Our model agrees reasonably well with experiments observing partial budding of retroviruses including HIV.

DOI: 10.1103/PhysRevE.78.051903 PACS number(s): 87.16.dr, 87.15.bk, 87.19.xd

I. INTRODUCTION

The human immunodeficiency virus (HIV) is famous for its ability to induce acquired immunodeficiency syndrome (AIDS). It belongs to a large family of enveloped RNA viruses, retroviruses. Retroviruses are characterized by the unique infection strategy of reverse transcription, in which the genetic information flows from RNA back to DNA (therefore the name "retro") [1]. Budding is an indispensable step in the retroviral life cycle [2,3]. After the major retroviral structural protein, Gags (originally mean group-specific AntiGens), are synthesized inside the host cell, they are transported to the cell membrane and self-assemble into spherical protein shells called "capsids," with viral RNA genome and other auxiliary viral proteins packaged inside. At the same time, these capsids, enveloped by the cellular membrane, must bud out of the membrane to target other host cells. In other words, budding and assembly of retroviruses happen *concurrently* on the cell membrane. Despite a large body of experiments done within the last decade, the biological pathway and mechanism of retroviral budding have still not been fully understood [2,3]. One important unexplained observation is that viral budding can be inhibited partially or completely by modifying the Gag proteins or changing the cell environment. In these situations, capsids are only partially formed and stuck on the membrane (Fig. 1). Motivated directly by this partial budding phenomenon, in this paper, we propose a physical model to study HIV (and retroviruses in general) budding and assembly on the elastic membrane. Physically, this problem is interesting because it provides a unique two-dimensional self-assembly mechanism in which the membrane elastic energy plays an important role, since assembly is always accompanied with budding. Biologically, understanding the physical mechanism of HIV budding and assembly is certainly important toward understanding the HIV life cycle. It is even more important in the light of recent effort from the virology community to develop assembly oriented antiviral therapy.

Budding of regular enveloped viruses was studied theoretically by Tzlil, Deserno, Gelbart, and Ben-Shaul (TDGB) in Ref. [5] (see also [6,7]). However, the viral budding pathway and the physical model studied by TDGB is qualitatively different from retroviral budding we study in this paper. For regular enveloped viruses, viral capsids are fully assembled inside the cell [8–11]. After that, they are transported to the cell membrane, bind to the viral spike proteins (embedded in the cell membrane), and then bud out through

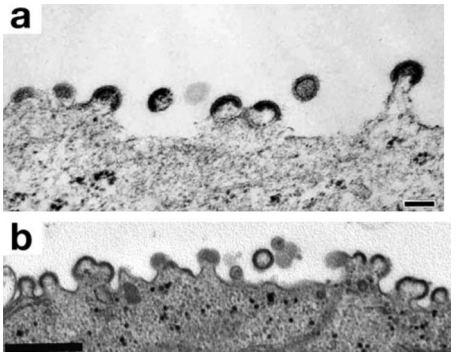

FIG. 1. Electron microscopic images of partial budding of HIV-1 viruses. (a) Reprinted from Ref. [2], with permission by Annual Reviews. Bar: 100 nm. (b) Reprinted from Ref. [4], with permission by Journal of Virology. Bar: 500 nm.

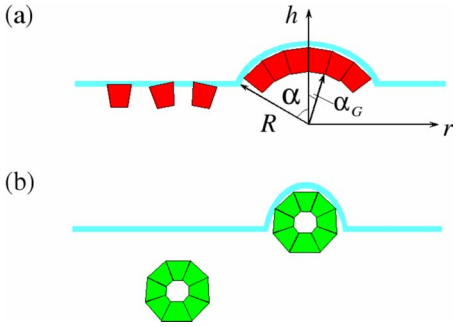

FIG. 2. (Color online) Schematic illustrations of two different types of virus budding. (a) Budding of retroviruses. Capsid proteins (Gags) are first attracted to the membrane, then self-assemble and bud on the membrane at the same time. This is the system studied in this paper. (b) Budding of regular enveloped viruses. Capsid proteins first self-assemble into complete capsids inside the cell, then bud on the membrane [5]. (a) Also shows the cylindrical coordinate system (r,h,ϕ) used in the model (the azimuthal angle ϕ is not shown).

the cell membrane [see Fig. 2(b)]. Therefore, capsids formation and budding out of the membrane are two separate processes. The main driving force of budding is the capsid-membrane attraction (mediated by embedded spike proteins).

Budding of retroviruses follows a completely different pathway. Various transmission electron microscopy and x-ray tomography experiments suggest that retroviral capsids are assembled from Gag proteins on the cell membrane and bud out of the cell *concurrently* [2,3]. Based on these experiments, we study a different model for HIV (and retrovirus in general) budding and assembly shown in Fig. 2(a). In this model, we assume retroviral capsids are assembled from membrane-bound Gags only, neglecting the possibility that Gags from the interior of the cell may participate. In other words, the Gag-membrane attraction is strong such that Gags always bind to the membrane. This assumption is supported by various experimental observation where budding is completely inhibited (no capsids are formed) but Gags are found in abundance at the cell membrane [12]. In contrast to the TDGB model, the primary driving force of our retroviral budding is the short-range attraction between these membrane-bound Gag proteins. This correlates well with the experimental fact that point mutations changing Gag-Gag interactions affect the degree of viral budding. On the other hand, spike proteins or virus RNA seem not important for retroviral budding. In vitro, Gag proteins are directly attracted to the membrane and they alone are usually sufficient for the assembly and release of viruslike particles [3,13,14]. We therefore neglect the contribution of all other proteins or RNA components of retroviruses in our model.

In this paper, for a given set of parameters (the membrane Gag concentration, the Gag-Gag interaction, and the cell membrane bending and stretching rigidity), we study the free energy profile of budded viral capsids. Two energies are considered explicitly: First, the elastic energy of the membrane including the bending and stretching energy; second, the Gag-Gag attraction energy when a Gag makes contact to the other Gag [see Fig. 2(a)]. Since the elastic energy scale is much larger than k_BT, for example, the bending rigidity of

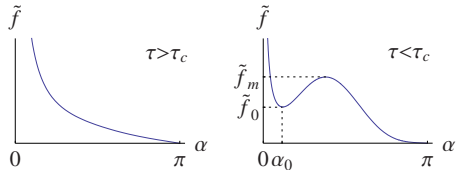

FIG. 3. (Color online) The schematic illustration of the total free energy density as a function of the capsid size α. The left- and right-hand profiles correspond to strong or weak Gag-Gag attraction, respectively. Here τ is the line tension of the rim of a partially budded capsid. τ is proportional to the strength of Gag-Gag attraction. τ_c is the threshold line tension at which the local minimum at α_0 appears.

normal membranes is about $20k_BT$, thermal fluctuations of the membrane are higher-order corrections and neglected in the theoretical treatment. Focusing on the budding process, we also assume that the Gag-Gag interaction is strong enough such that the entropic cost of bringing free Gags to the capsid can be ignored. For simplicity, we assume the shape of the capsid together with the membrane attached to it is (partially) spherical with radius R [Fig. 2(a)]. The size of a capsid is then characterized by the zenith angle α at its edge, the smallest being the angle of a single Gag protein, α_G [Fig. 2(a)]. Since α_G is very small (α_G=0.03 for a typical HIV capsid containing 5000 Gags), we take $\alpha_G \to 0$ in the theoretical consideration and treat α as a continuous variable. As budding proceeds to completion, α increases from α_G to π. When $\alpha=\pi$, the capsid actually leaves the membrane through membrane fission. In this paper, we do not consider this fission process and thus, in our terminology, complete budding always means $\alpha \to \pi$. To simplify the calculation, we employ a scaling description where we neglect the variation in the degree of viral budding and assume all capsids have the same average zenith angle α.

Our main result is shown in Fig. 3. The key parameter is the strength of Gag-Gag attraction which can be adjusted experimentally by mutating Gags, complexing Gags with other molecules or by changing pH or salinity of the cell cytoplasm near the membrane [2,15]. In a partially budded capsid, the line tension τ of the rim of a capsid is directly proportional to this Gag-Gag interaction. When the Gag-Gag attraction is strong (or when τ is greater than a threshold value τ_c), as in the normal biological conditions of HIV, budding always proceeds to completion, i.e., $\alpha \to \pi$ (the left-hand panel of Fig. 3). At the early stage of budding, the size of a partially budded capsid increases very slowly with time,

$$\alpha(t) \approx (t/\tau_{\text{diff}})^{1/2}, \tag{1}$$

where the time scale τ_{diff} depends on the lateral mobility of the Gag, the radius of the capsid and the initial concentration Gag [see Eq. (51)]. On the other hand, when the Gag-Gag attraction is weak ($\tau < \tau_c$), for example, after mutation of the late domains of the Gag protein, partial budding appears as a metastable state at the capsid size α_0 (the right-hand panel of Fig. 3). In this case, the free energy barrier can be much larger than k_BT and budding is kinetically trapped at α_0. Using a linear approximation, we find

$$\alpha_0 \simeq \sqrt[4]{\frac{\tau^2}{\kappa\sigma}}, \tag{2}$$

where σ and κ are the surface tension and bending rigidity of the membrane.

The energetics of HIV budding and assembly is studied both analytically and numerically in this paper. Analytically, the complete scaling behaviors of the free energy density profile in asymptotic limits of "soft" and "stiff" membranes are calculated (the meaning of "soft" and "stiff" membrane will be clear in the later sections). In all cases, they agree well with the numerical result. On the other hand, the numerical result gives a complete solution to the problem including nonlinear regimes where the analytical result is normally not available. The inequality $\alpha_0 < 0.3\pi$ is found to always hold from the numerical calculation without any approximations.

It is worth to point out that budding in our model can be considered as a consequence of the inhomogeneity of the membrane if one considers Gags as a part of the membrane. In this sense, our work is related to the work of Jülicher and Lipowsky on domain-induced budding of vesicles [16,17]. However, in their papers, the inhomogeneity was introduced through two kinds of lipids which do not carry a given curvature like our Gags. Domain-induced budding is a consequence of demixing of these different molecules. As a result, their budding happens in a much larger length scale (comparable to the size of the vesicle) where only two phases coexist, one budded out from the other. While in our case, we consider budding at a much smaller length scale (a typical HIV-1 virus particle is about 140 nm in diameter, which is 100 times smaller than the size of a host cell) and there is a multiphase coexistence in the system since there are more than one capsid on the membrane.

This paper is organized as follows. In Sec. II, we introduce the physical model of HIV budding and assembly. We then discuss the analytical solution to the elastic energy of the membrane in Sec. III and to the total free energy density in Sec. IV. The numerical result is then provided and compared to the analytical results in Sec. V. After we get the complete theoretical result, we discuss budding kinetics and make connections to experiments in Sec. VI. We finally conclude in Sec. VII. In this paper, the term "capsid" is used for both partial and complete spherical shells of viral proteins. The meaning should be clear from the context.

II. ELASTIC MODEL OF HIV CAPSID BUDDING AND SELF-ASSEMBLY

Let us consider a membrane-capsid system in which the concentration of Gags on the membrane, c_G, is fixed. We assume all capsids assembled by Gags have the same average zenith angle α [see Fig. 2(a)], and an average concentration, n. n is related to α by the conservation of mass of Gags,

$$n = c_G \frac{A(\alpha_G)}{A(\alpha)} = c_G \frac{1-\cos\alpha_G}{1-\cos\alpha}, \tag{3}$$

where

$$A(\alpha) = 2\pi R^2 \int_0^\alpha \sin\theta d\theta = 2\pi R^2 (1-\cos\alpha) \tag{4}$$

is the area of a capsid with zenith angle α, and α_G is the zenith angle of a single Gag [see Fig. 2(a)]. Within this scaling description, it is convenient to think that the whole membrane surface is divided into identical cells, each contains a single capsid. The average size of these approximately circular cells, d, is given by the condition

$$\pi(d/2)^2 n = 1. \tag{5}$$

Generically, the free energy density of the membrane-capsid system can be written as

$$f = n\varepsilon = n(\varepsilon_m + \varepsilon_c), \tag{6}$$

where ε is the free energy of one membrane cell. It includes two parts: The elastic energy of the membrane, ε_m, and the capsid energy ε_c coming from the Gag-Gag interaction and the Gag-membrane interaction.

To calculate the elastic energy of the cell membrane, we use the standard Helfrich model [18,19] where ε_m is the sum of two contributions from the bending energy and the stretching energy,

$$\varepsilon_m = \int dS \left(\frac{\kappa}{2}(2H - C_0)^2 + \kappa_G K \right) + \int dS\sigma. \tag{7}$$

Here the integration with the area element dS is taken over the membrane surface. κ and κ_G are the bending rigidity and Gaussian bending rigidity, H and K are the mean and Gaussian curvatures, and C_0 is the spontaneous curvature of the membrane surface. Using the Gauss-Bonnet theorem, one can show that the total Gaussian curvature of the membrane surface is proportional to the total area of capsids, even in the generic case when κ_G takes different values for the membrane attached to the capsid and the Gag-free membrane. Since the Gag concentration c_G in our system is fixed, this term gives a constant in f and can be dropped from further consideration [20]. For a given Gag concentration c_G, under our spherical capsid assumption, the shape and the total area of all capsids are fixed. Therefore, the total elastic energy of the membrane attached to capsids is also constant, and can also be dropped from consideration. As a result, the α-dependent contribution to ε_m comes from the integration over the Gag-free membrane surface only. In this region, we take the spontaneous curvature to be $C_0 = 0$, corresponding to normal lipid bilayer membranes.

In consideration of the single capsid energy ε_c, since c_G is constant, both the total Gag-membrane interaction energy and the bulk part of the Gag-Gag interaction energy are constant. The only α-dependent contribution to ε_c comes from the rim energy of the capsid, due to the fact that the coordination number of Gags on the rim is not as many as Gags inside the capsid. Since the perimeter of the capsid rim with zenith angle α is $2\pi R \sin\alpha$, we set

$$\varepsilon_c = \tau 2\pi R \sin\alpha. \tag{8}$$

The proportionality coefficient τ can be considered as the "line tension" of the capsid. It is directly proportional to the

strength of the Gag-Gag attraction and can be changed experimentally by modification of Gags or by changing pH or salinity of the cell cytoplasm near the membrane.

To proceed further, we take the "ideal capsids" approximation when the distance between capsids is large and the membrane mediated interaction between them is negligible. Such an effective long-range interaction is possible because the presence of the first capsid may change the deformation of the membrane around the second capsid and provides an effective interacting energy between the two. Qualitatively, this interaction is negligible when the capsid concentration n is small (the quantitative condition will be given in the next section). Under this noninteracting capsids approximation, ε_m comes from the membrane deformation induced by a single capsid.

The calculation procedure to find the free energy profile $f(\alpha)$ is as follows. We first minimize the membrane elastic energy ε_m with respect to all possible membrane shapes for any given capsid size α. Here it is convenient to use a cylindrical coordinate system (r,h,ϕ) as shown in Fig. 2(a) (the azimuthal angle ϕ is not shown). With our assumption of (partial) spherical capsids, the membrane profile is independent on ϕ. As a result, one can use either the function $h(r)$ or $r(h)$ to parametrize the membrane. Correspondingly, the mean curvature and the area element can be written as [21]

$$H(r) = \frac{h'(r)^3 + h'(r) + rh''(r)}{2r[1 + h'(r)^2]^{3/2}}, \tag{9}$$

$$dS = r\sqrt{1 + h'(r)^2}drd\phi; \tag{10}$$

or

$$H(h) = \frac{1 + r'(h)^2 - r(h)r''(h)}{2r(h)[1 + r'(h)^2]^{3/2}}, \tag{11}$$

$$dS = r(h)\sqrt{1 + r'(h)^2}dhd\phi, \tag{12}$$

where $h'(r)=dh/dr$ and $h''(r)=d^2h/dr^2$ are the first and second derivatives of h with respect to r. Similarly, $r'(h)=dr/dh$ and $r''(h)=d^2r/dh^2$ are the first and second derivative of r with respect to h. Functionally minimizing the membrane energy ε_m with respect to membrane shape $r(h)$ or $h(r)$, one obtains an elastic equation of the membrane shape, similar to the Euler-Lagrange equation derived from the least action principle in the classical mechanics. For the shape parametrization using $r(h)$, $\delta\varepsilon_m/\delta r=0$ leads to the equation

$$\begin{aligned}\frac{\kappa}{2r^2(1+r'^2)^{9/2}}&(-r'^2 - 3r'^4 - 3r'^6 - r'^8 + rr'' - 3rr'^4r'' \\ &- 2rr'^6r'' + 2r^2r''^2 - 11r^2r'^2r''^2 - 13r^2r'^4r''^2 - 5r^3r''^3 \\ &+ 30r^3r'^2r''^3 + 4r^2r'r^{(3)} + 8r^2r'^3r^{(3)} + 4r^2r'^5r^{(3)} \\ &- 20r^3r'r''r^{(3)} - 20r^3r'^3r''r^{(3)} + 2r^3r^{(4)} + 4r^3r'^2r^{(4)} \\ &+ 2r^3r'^4r^{(4)}) + \sigma\frac{1 + r'^2 - rr''}{(1+r'^2)^{3/2}} = 0,\end{aligned} \tag{13}$$

where $r^{(3)}=d^3r/dh^3$ and $r^{(4)}=d^4r/dh^4$ are the third and fourth derivatives of r with respect to h. This equation must be solved together with the boundary conditions. On the rim of the partial spherical capsid, the membrane itself and its slope must be continuous. We have

$$h(r)|_{R\sin\alpha} = R\cos\alpha, \quad h'(r)|_{R\sin\alpha} = -\tan\alpha, \tag{14}$$

or

$$r(h)|_{R\cos\alpha} = R\sin\alpha, \quad r'(h)|_{R\cos\alpha} = -\cot\alpha. \tag{15}$$

Far away from the capsid, the membrane becomes flat. We have

$$h'(r)|_{\infty} = 0 \tag{16}$$

or

$$r'(h)|_{\infty} = \infty. \tag{17}$$

Solving the elastic equation (13) with the boundary conditions, Eq. (15) and (17) [or Eq. (14) and Eq. (16) if $h(r)$ is used], one obtains the membrane shape that minimizes ε_m. Substituting this shape into Eq. (7), one obtains the minimal $\varepsilon_m(\alpha)$. Setting its value into Eq. (6), one gets the total free energy density profile $f(\alpha)$. In general, the elastic equation, Eq. (13), is highly nonlinear and numerical calculations are needed to obtain the exact membrane profile, as shown in Sec. V. However, in certain asymptotic limits, analytical solutions can be obtained which determine the scaling behavior of the system. This is done in the next two sections.

III. ASYMPTOTIC SOLUTIONS OF THE MEMBRANE ELASTIC ENERGY

In calculating the free energy profile, the most nontrivial part is to find the minimal $\varepsilon_m(\alpha)$, due to the nonlinear elastic equation involved. After the solution is found, it is straightforward to add the other part of the energy $\varepsilon_c(\alpha)$ and obtain $f(\alpha)$. Therefore, we focus on the solution of minimal ε_m in this section. Although not solvable in general, the problem does have analytical solutions in asymptotic limits. To a large extent, they determine the analytical behavior of the system, especially the scaling behavior of ε_m with the dimensionless parameter

$$\tilde{\sigma} = R\sqrt{\frac{\sigma}{\kappa}}, \tag{18}$$

which characterize the relative strength of the surface tension to the bending rigidity.

A. Small deformation solution

A typical approach to consider the elastic deformation of the membrane is to take the small deformation approximation which assumes $|\nabla h| \ll 1$ [22]. Here we use the notation

$$\nabla = \hat{r}\partial_r + \hat{\phi}\frac{1}{r}\partial_\phi \tag{19}$$

in order to show similarity of the elastic equation to the linearized Poisson-Boltzmann equation later. Expanding with ∇h and keeping terms of $O(\nabla h)^2$ in $\delta\varepsilon_m=0$, we reach a lin-

earized elastic equation which can be written as

$$H = \frac{1}{2}\nabla^2 h,$$

$$\nabla^2 H - \frac{H}{r_s^2} = 0, \tag{20}$$

where we have introduced an important length scale in the problem,

$$r_s = \sqrt{\frac{\kappa}{\sigma}}. \tag{21}$$

It is the length scale beyond which the stretching energy becomes more important than the bending energy. Notice that Eq. (20) takes exactly the same form as a linearized Poisson-Boltzmann equation in electrolytes or plasma [23]. Therefore, r_s can be interpreted as an elastic screening length, similar to the Debye-Hückel screening radius. The local curvature $H(r)$ induced by the capsid decreases when r increases and becomes exponentially small at distance larger than r_s. This is a typical linear solution of small deformation.

Using boundary conditions Eqs. (14) and (16), the special solution to Eq. (20) is given by

$$h(r) = R\cos\alpha + r_s \tan\alpha \frac{K_0(r/r_s) - K_0(R\sin\alpha/r_s)}{K_1(R\sin\alpha/r_s)}, \tag{22}$$

$$h'(r) = -\tan\alpha \frac{K_1(r/r_s)}{K_1(R\sin\alpha/r_s)}, \tag{23}$$

$$H(r) = \frac{\tan\alpha}{2r_s}\frac{K_0(r/r_s)}{K_1(R\sin\alpha/r_s)}, \tag{24}$$

where K_0 and K_1 are the zero- and first-order modified Bessel function of the second kind. At $r \gg r_s$, both $K_0(r/r_s)$ and $K_1(r/r_s)$ decay like $\sqrt{r_s/r}\exp(-r/r_s)$, and the deformation becomes exponentially small, as the meaning of r_s suggested.

Substituting this solution back to Eq. (7), we get the minimal elastic energy of the membrane

$$\varepsilon_m = \pi\kappa \tan^2\alpha \frac{R\sin\alpha}{r_s}\frac{K_0(R\sin\alpha/r_s)}{K_1(R\sin\alpha/r_s)}. \tag{25}$$

Notice that this energy is proportional to the dimensionless parameter $\tilde{\sigma} = R\sqrt{\sigma/\kappa} = R/r_s$. Here, the inverse proportion to r_s is again a generic feature shared with the theory of Debye-Hückel linear screening [23].

The self-consistency of the small deformation approximation is warranted by $|h'(r)| < 1$, or, according to Eq. (23), $|\tan\alpha| < 1$. Therefore, this solution is applicable in the whole range of r for $\alpha < \pi/4$ capsids only. On the other hand, at large distances far away enough from the capsid, the deformation of the membrane always becomes small enough such that the small deformation solution is applicable. In this sense, this solution can always serve as a "far-capsid" solution for the membrane shape, although the formula for ε_m in Eq. (25) is not valid in general. It describes the universal decaying behavior of the deformation when the deformation itself becomes small enough. We can formally define a characteristic distance r_c through

$$|h'(r_c)| = 1, \tag{26}$$

beyond which the small deformation solution is valid. r_c will be useful later when we discuss the complete solution to the problem.

With the small deformation solution in hand, we are now ready to derive a quantitative condition for the ideal capsid approximation introduced in the last section. Clearly, when the average projected distance between capsids, d_0, is much larger than $r_s + 2R$, the membrane mediated interaction between capsids is negligible, since the deformations of the membrane by the capsids at distance larger than r_s are screened out. In this case, most of the membrane surface is flat, so $d_0 \simeq d$ (notice that d is measured along the membrane surface which in general is larger than d_0 measured along r axis). Thus according to Eqs. (3) and (5), the ideal capsids approximation is valid when

$$\frac{d_0}{r_s + 2R} = \frac{2\sin(\alpha/2)}{(r_s + 2R)\sqrt{\pi c_G}\sin(\alpha_G/2)} \gg 1. \tag{27}$$

In this work, we assume c_G is small enough and this is always the case. Using relevant parameters for HIV (see Sec. VI for more details), this approximation is valid when c_G is less than 0.1 nm^{-2}.

B. Catenoid solution

When the surface tension $\sigma = 0$ or $r_s \to \infty$, again an analytical solution is available [24,25]. In this case, the second integral in Eq. (7) is zero. Our problem of finding the minimal ε_m is reduced to a minimal surface problem in differential geometry [21]. Namely, we look for the solution to the equation $H = 0$ [26]. The only solution under the rotational symmetry of our problem is the catenoid solution, first discovered by Euler in 1740 [27].

In this case, due to the possible multiple values of h at the same r, it is better to use the $r(h)$ parametrization. H is then given by Eq. (11). Using boundary conditions (15) and (17), the special solution to $H = 0$ is

$$r(h) = R\sin^2\alpha \times \cosh\frac{h - R\cos\alpha - R\sin^2\alpha\,\text{arcsinh}(\cot\alpha)}{R\sin^2\alpha}. \tag{28}$$

The catenoid shapes near the capsids are illustrated in the upper panels of Fig. 4. In this catenoid shape, the elastic energy ε_m achieves its absolute minimum, zero.

The catenoid solution is a solution to a nonlinear differential equation. It involves large deformations which cannot be characterized by the linear solution discussed in the preceding subsection. Although exact only when $r_s \to \infty$, this solution is still useful for large but finite r_s [28]. In fact, since there are no other length scales in the elastic equation (13) (R only shows up in the boundary conditions), a large r_s actually means $r_s \gg r$. Therefore, in the region of $r \ll r_s$, the catenoid solution should work asymptotically. In this sense, this solution can always serve as a "near-capsid" solution for the

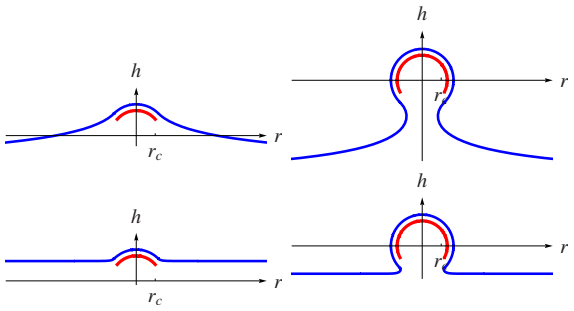

FIG. 4. (Color online) Numerical result of the optimal membrane shape (dark gray, blue online) around a capsid (light gray, red online). The upper panels are plotted in the "soft membrane" regime. $\tilde{\sigma}=0.1$ or $r_s=10R$. Here the membrane takes the catenoid shape. The lower panels are plotted in the "stiff membrane" regime. $\tilde{\sigma}=10$ or $r_s=0.1R$. The left-hand panels are plotted at $\alpha=0.25\pi$. The right-hand panels are plotted at $\alpha=0.75\pi$. r_c are shown for comparison with corresponding r_s.

membrane shape, although $\varepsilon_m=0$ is not true in general. The characteristic length beyond which it fails is simply r_s.

In the case of $r_s\to\infty$ and $\alpha\ll 1$, both the catenoid solution and the small deformation solution work in all ranges of r. Indeed they become identical.

C. Membrane elastic energy at two asymptotic limits

The two solutions discussed in the last two subsections determine the analytical behavior of the system to a large extent. They determine the scaling behavior of ε_m with respect of $\tilde{\sigma}$. When $\tilde{\sigma}\ll 1$, they can even be combined to get the analytical expression of the minimal ε_m. Below we separate our discussion into two opposite limits of small and large $\tilde{\sigma}$, which can be called the soft membrane regime and the stiff membrane regime. Here "soft" means easy to stretch, "stiff" means the opposite. See Fig. 4 for a direct illustration of the "soft" or "stiff" membranes.

In the soft membrane regime, $\tilde{\sigma}\ll 1$ or $R\ll r_s$, the catenoid solution is valid near the capsid when $r\ll r_s$. Calculating r_c using Eqs. (28) and (26), we obtain

$$r_c=\sqrt{2}R\sin^2\alpha. \tag{29}$$

We see $r_c\ll r_s$. Therefore, the valid regions of the two asymptotic solutions (one is $r>r_c$, the other is $r<r_s$) overlap largely and we can combine them to get a complete solution to the optimal membrane shape. Quantitatively, we artificially choose a projected distance somewhere between r_c and r_s, say $\sqrt{r_c r_s}$. For $r<\sqrt{r_c r_s}$, the catenoid solution is used. For $r>\sqrt{r_c r_s}$, the small deformation solution is used. Notice that the special solution of the small deformation now must be calculated using the continuity conditions for $h(r)$ and $h'(r)$ at $\sqrt{r_c r_s}$, derived from the catenoid solution. As a result, we have an analytical expression for the optimal membrane shape continuously from the edge of the capsid to infinity (see the upper panels of Fig. 4 plotted using the numerical result which agrees with the analytical calculation). The corresponding ε_m, keeping the leading order terms in the small parameter $\tilde{\sigma}$, is given by

$$\varepsilon_m=\pi\kappa\sin^4\alpha\frac{R^2}{r_s^2}\ln\frac{r_s}{R}. \tag{30}$$

We see $\varepsilon\propto\tilde{\sigma}^2\ln(1/\tilde{\sigma})$. When $\alpha\ll 1$, this result agrees with the small deformation solution in Eq. (25) in the same regime of small $\tilde{\sigma}$.

In the stiff membrane regime, $\tilde{\sigma}\gg 1$ or $R\gg r_s$. Since $r\gg r_s$ always, the "near capsid" region where the catenoid solution holds disappears. On the other hand, for $\alpha<\pi/4$, the small deformation solution is valid in the whole range of r. The membrane elastic energy is given by (25), which in this limit reads as

$$\varepsilon_m=\pi\kappa\tan^2\alpha\sin\alpha\frac{R}{r_s}. \tag{31}$$

For $\alpha>\pi/4$ capsids, a rough estimate of r_c using Eq. (23) gives

$$r_c\simeq R\sin\alpha+r_s\ln|\tan\alpha|. \tag{32}$$

Since $R\gg r_s$, for most of α, we expect that the small deformation solution starts to work at places close to the capsid (see the lower panels of Fig. 4 plotted using the numerical result). Probably because of this, the scaling behavior of $\varepsilon_m\propto\tilde{\sigma}$ is preserved even at large α, as shown by the numerical result (see Sec. V).

IV. ANALYTICAL RESULT OF THE TOTAL FREE ENERGY DENSITY

After the information about the minimal $\varepsilon_m(\alpha)$ is known, we can add the line tension energy $\varepsilon_c(\alpha)$ to it and consider the total free energy density $f(\alpha)$. The presence of ε_c introduces the second dimensionless parameter to the problem,

$$\tilde{\tau}=\frac{R\tau}{\kappa}, \tag{33}$$

which characterizes the relative strength of the line tension on the capsid rim. In this section, we derive several simple scaling behaviors of the system, depending on the two dimensionless parameters $\tilde{\sigma}$ and $\tilde{\tau}$. We again separate our discussion into the soft and stiff membrane regimes corresponding to small and large $\tilde{\sigma}$.

A. Soft membrane regime

In the soft membrane regime, $\tilde{\sigma}=R/r_s\ll 1$. Substituting Eqs. (8) and (30) to Eq. (6), we have

$$f\equiv\kappa c_G(1-\cos\alpha_G)\tilde{f}=\kappa c_G(1-\cos\alpha_G)\pi\cot\frac{\alpha}{2}\times\left(2\tilde{\tau}+\tilde{\sigma}^2\ln\frac{1}{\tilde{\sigma}}\sin^3\alpha\right), \tag{34}$$

where we have introduced the dimensionless free energy density $\tilde{f}$ for convenience. $\tilde{f}(\alpha)$ is plotted schematically in Fig. 3. When $\tilde{\tau}$ is large, the only minimum of the free energy density is at $\alpha\to\pi$ (the left-hand panel of Fig. 3). On the other hand, when $\tilde{\tau}<0.2\tilde{\sigma}^2\ln(1/\tilde{\sigma})$, a local minimum at the

capsid size, α_0, appears (the right-hand panel of Fig. 3). Correspondingly, the threshold line tension at which the local minimum in the free energy density appears is

$$\tau_c = 0.2R\sigma \ln \frac{1}{R\sqrt{\sigma/\kappa}}. \tag{35}$$

Since transcendental equations are involved in minimization of $\tilde{f}$, it is not easy to get the analytical expression about this local minimum in general. However, α_0 and the corresponding $\tilde{f}_0$ can be estimated in a linear approximation. Assuming α_0 is achieved at small α, we can expand $\tilde{f}$ and keep only the leading order terms in α. We obtain

$$\tilde{f} = \frac{4\pi\tilde{\tau}}{\alpha} + 2\pi\tilde{\sigma}^2 \ln \frac{1}{\tilde{\sigma}}\alpha^3. \tag{36}$$

Taking $\partial f/\partial\alpha = 0$, we have

$$\alpha_0 = \sqrt[153]{\frac{\tilde{\tau}}{\tilde{\sigma}^2 \ln(1/\tilde{\sigma})}} = \sqrt[153]{\frac{\tau}{R\sigma \ln(\sqrt{\kappa/\sigma}/R)}}. \tag{37}$$

The fact that this is a minimum rather than a maximum is confirmed by $\partial^2\tilde{f}/\partial\alpha^2|_{\alpha_0} > 0$. For $\tau < \tau_c$ at which α_0 shows up, this result is indeed much smaller than 1, consistent with the initial assumption that $\alpha_0 \ll 1$. In the same limit,

$$\tilde{f}_0 \simeq 4\pi\sqrt[4]{\tilde{\tau}^2\tilde{\sigma}^2 \ln(1/\tilde{\sigma})} = 4\pi\frac{R}{\kappa}\sqrt[153]{\tau^2\sigma \ln\frac{\sqrt{\kappa/\sigma}}{R}}. \tag{38}$$

B. Stiff membrane regime

In this case, we do not know the form of the membrane elastic energy ε_m for large α. Still, in the same spirit of linear analysis, we can assume that there is a minimum of f at small α, and use the small deformation solution Eq. (31) for ε_m. Notice that the minimum found in this way is only a local minimum, since we did not include the information of large α.

As a result, we have

$$\tilde{f} = \pi \cot\frac{\alpha}{2}(2\tilde{\tau} + \tilde{\sigma}\tan^2\alpha) \simeq \frac{4\pi\tilde{\tau}}{\alpha} + 2\pi\tilde{\sigma}\alpha. \tag{39}$$

Taking $\partial f/\partial\alpha = 0$, we obtain

$$\alpha_0 = \sqrt{\frac{2\tilde{\tau}}{\tilde{\sigma}}} = \sqrt[4]{\frac{4\tau^2}{\kappa\sigma}}. \tag{40}$$

It is a minimum since $\partial^2\tilde{f}/\partial\alpha^2|_{\alpha_0} > 0$. For this result to be meaningful, $\tilde{\tau} \ll \tilde{\sigma}$ must hold, which will be checked in comparison with the numerical result. The corresponding free energy density is

$$\tilde{f}_0 = 4\pi\sqrt{2\tilde{\sigma}\tilde{\tau}} = 4\pi R\sqrt[4]{\frac{4\sigma\tau^2}{\kappa^3}}. \tag{41}$$

V. NUMERICAL RESULT AND DISCUSSION

In order to verify our analytical understanding and get the complete solution to the problem, we solve the nonlinear elastic equation derived from $\delta\varepsilon_m = 0$ numerically. Our computation procedure follows Refs. [7,29]. This numerical solution is then combined with ε_c to give the total free energy density f. In this section, we show the numerical result, compare it with the analytical formulas, and discuss the meaning of our results.

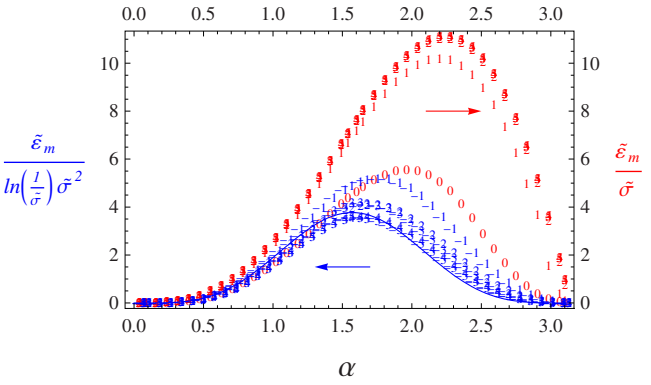

FIG. 5. (Color online) Numerical result of the dimensionless membrane elastic energy $\tilde{\varepsilon}_m = \varepsilon_m/\kappa$ as a function of α. The 11 sets of data points are at $\tilde{\sigma} = 10^{-5}, 10^{-4}, 10^{-3}, \ldots, 10^{5}$. They are labeled correspondingly as $-5, -4, -3, \ldots, 5$. The right axis $\tilde{\varepsilon}_m/\tilde{\sigma}$ is for all $\tilde{\sigma} \geqslant 1$ data points (light gray, red online), while the left axis $\tilde{\varepsilon}_m/\tilde{\sigma}^2 \ln(1/\tilde{\sigma})$ is for all $\tilde{\sigma} < 1$ data points (dark gray, blue online), as indicated by the two arrows. The curve represents the analytical asymptotic solution (30) with an additional factor 1.3 (dark gray, blue online), fitting the data points for $\tilde{\sigma} \ll 1$.

The direct numerical result of ε_m is plotted in Fig. 5, where for convenience we used the dimensionless elastic energy $\tilde{\varepsilon}_m = \varepsilon_m/\kappa$. The first important thing to notice is that the elastic energy profile always takes a "sand dune" shape, where two minimums, zeros, are achieved at $\alpha \to 0, \pi$, and a maximum shows up in the middle of α. Physically, this energy profile comes from the need of matching boundary conditions at the edge of the capsid and at infinity. The membrane deformed by the capsid edge at one end must become flat far away from the capsid. At $\alpha \to 0$ and $\alpha \to \pi$, the membrane is not deformed at all, and the elastic energy is zero [30]. While for α close to $\pi/2$, the membrane is almost vertical at the edge of the capsid, and a large amount of elastic energy is needed to bend it flat.

Second, we see clearly two kinds of asymptotic behaviors of ε_m depending on the parameter $\tilde{\sigma} = R/r_s$. In the stiff membrane regime, $\tilde{\sigma} \gg 1$, the energy is proportional to $\tilde{\sigma}$ as shown by the collapse of the data points to a single curve with $\tilde{\sigma}$ varying from 10^2 to 10^5. The maximum of the energy is achieved at $\alpha_m \simeq 0.7\pi$. α_m is a nonlinear result and cannot be calculated analytically. However, the proportionality of ε_m to $\tilde{\sigma}$ is a small deformation result as shown in Eq. (31). In the soft membrane regime, $\tilde{\sigma} \ll 1$, the energy is proportional to $\tilde{\sigma}^2 \ln(1/\tilde{\sigma})$, shown again by the collapse of the data points with $\tilde{\sigma}$ varying from 10^{-2} to 10^{-5}. Here the collapse is not as pronouncing as in the other regime mostly due to the larger numerical error in dealing with smaller $\tilde{\varepsilon}_m$. The absolute value of $\tilde{\varepsilon}_m$ in this regime is smaller at least in four orders of magnitude than in the other regime. The maximum of the energy here is arrived at $\alpha_m = \pi/2$ and the curve becomes symmetric about α_m. These features agree with our small $\tilde{\sigma}$

solution originating from the catenoid solution. In fact, Eq. (30) fits the numerical data reasonably well, with an additional factor 1.3. The qualitative difference between the soft and stiff membrane regimes can also be seen directly from the optimal membrane shape minimizing the membrane elastic energy around a capsid with a given size α, as shown in Fig. 4.

The scaling of ε_m with $\tilde{\sigma}$ suggests a simple way to do the numerical calculation to the free energy density. When $\tilde{\sigma} \gg 1$,

$$\tilde{f} = \tilde{\varepsilon}_c + \tilde{\varepsilon}_m = 2\pi \cot\frac{\alpha}{2}\tilde{\tau} + g_1(\alpha)\tilde{\sigma} = \tilde{\sigma}\left(2\pi \cot\frac{\alpha}{2}\frac{\tilde{\tau}}{\tilde{\sigma}} + g_1(\alpha)\right), \tag{42}$$

where $\tilde{\varepsilon}_c = \varepsilon_c/\kappa$ and $g_1(\alpha)$ is some function given by the numerical computation. According to the last equality, up to an overall constant $\tilde{\sigma}$, $\tilde{f}$ is completely determined by only one parameter $\tilde{\tau}/\tilde{\sigma}$. Similarly, when $\tilde{\sigma} \ll 1$,

$$\tilde{f} = \tilde{\sigma}^2 \ln\frac{1}{\tilde{\sigma}}\left(2\pi \cot\frac{\alpha}{2}\frac{\tilde{\tau}}{\tilde{\sigma}^2 \ln(1/\tilde{\sigma})} + g_2(\alpha)\right), \tag{43}$$

where $g_2(\alpha)$ is again given by numerical computation, although we know it from our analytical result in Eq. (34). In this regime, $\tilde{f}$ is determined by one parameter $\tilde{\tau}/\tilde{\sigma}^2 \ln(1/\tilde{\sigma})$. Below in studying the local minimum of $\tilde{f}$, we therefore consider a single parameter dependence.

For all $\tilde{\sigma}$ and $\tilde{\tau}$, we get two different types of free energy density profiles as shown in Fig. 3, consistent with the analytical result for small $\tilde{\sigma}$. The global minimum of the free energy density is always at $\alpha \to \pi$. Physically, the line tension energy prefers the shortest length of the capsid rim, which is zero for complete capsids ($\alpha \to \pi$). When $\tilde{\tau}$ is very large, the line tension energy dominates, and the free energy density $\tilde{f}$ decreases with α monotonically to zero, as shown in the left-hand panel of Fig. 3. On the other hand, when $\tilde{\tau}$ is small, due to the maximum of the membrane elastic energy ε_m, a local minimum at the capsid size, α_0, shows up in the free energy density, as shown in the right-hand panel of Fig. 3. It is useful to draw a "phase diagram" on the plane of $\tilde{\sigma}$ and $\tilde{\tau}$ as in Fig. 6 to show this qualitative difference in the free energy density profile. The lower-right-hand region of Fig. 6 corresponds to value of the parameters $(\tilde{\sigma}, \tilde{\tau})$ where capsid budding can be kinetically trapped. The two lines fit the "phase boundary" at large and small $\tilde{\sigma}$ with $\tilde{\tau}=0.11\tilde{\sigma}$ and $\tilde{\tau}=0.065\tilde{\sigma}^2 \ln(1/\sigma)$, respectively. As one can see, there is a very good agreement between numerical results and our scaling formulas for $\tilde{\sigma}$ in two asymptotic limits. According to the numerical fits, the threshold τ at which the local minimum in the free energy density shows up are

$$\tau_c = 0.11\sqrt{\kappa\sigma} \tag{44}$$

when $\tilde{\sigma} \gg 1$, and

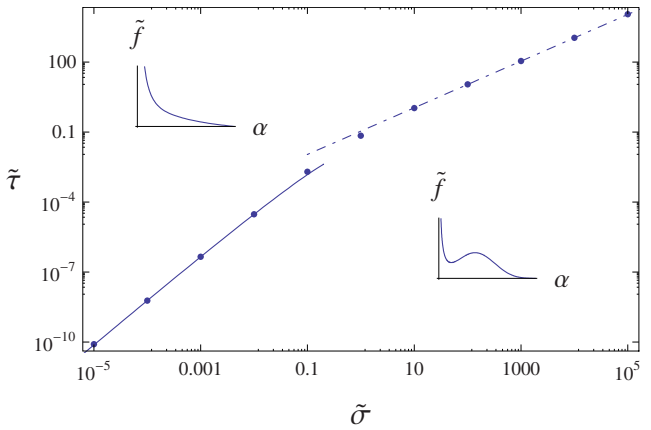

FIG. 6. (Color online) An effective "phase diagram" in the plane of two dimensionless parameters, $\tilde{\sigma}=R/r_s$ and $\tilde{\tau}=R\tau/\kappa$. In the upper-left-hand part, the free energy density decreases monotonically with α, while in the lower-right-hand part, it has a local minimum, as shown in the insets. The numerical data points mark the "phase boundary" at which the local minimum appears. The dotted-dashed line and the solid lines fit the data points using $\tilde{\tau}=0.11\tilde{\sigma}$ and $\tilde{\tau}=0.065\tilde{\sigma}^2 \ln(1/\tilde{\sigma})$, respectively.

$$\tau_c = 0.065R\sigma \ln\frac{1}{R\sqrt{\sigma/\kappa}} \tag{45}$$

when $\tilde{\sigma} \ll 1$. The later formula agrees with our analytical result in Eq. (35) with a numerical factor 3 difference.

The possible local minimum in $\tilde{f}$ (the right-hand panel in Fig. 3) suggests that budding may be trapped kinetically at the capsid size α_0. Numerical and analytical results of α_0 are shown in Fig. 7. The analytical curves are drawn using Eq. (40) at $\tilde{\sigma} \gg 1$ and Eq. (37) at $\tilde{\sigma} \ll 1$, with additional numerical factors of 2 and 1.5, respectively. There is some deviation between analytical and numerical results at large $\tilde{\tau}$. This is the parameter regime where the linear approximation is no longer valid.

The kinetic trapping becomes significant if the barrier in the free energy density is large. In Fig. 8, numerical and analytical results about this barrier are plotted. For the local minimum $\tilde{f}_0$, up to an order of one numerical factor (1.7 and 3.2), our analytical expressions Eq. (41) at $\sigma \gg 1$ and Eq. (38) at $\sigma \ll 1$ remains a reasonable approximation. We cannot estimate the maximum $\tilde{f}_m$, which is in the nonlinear regime. However, in the most important regime of small $\tilde{\tau}$ and large barrier, Fig. 8 shows that the main contribution to $\tilde{f}_m$ comes from the membrane elastic energy ε_m (the value of $\tilde{f}_m$ at $\tilde{\tau}=0$). In this regime, the additional contribution to $\tilde{f}_m$ from the line tension energy ε_c is negligible and $\tilde{f}_m$ is almost a constant. Combining the numerical result of $\tilde{f}_m$ and the analytical result of $\tilde{f}_0$ with proper numerical factors, we obtain the asymptotic formulas for the barrier at $\tilde{\tau} \ll 1$,

$$\tilde{f}_m - \tilde{f}_0 \simeq 7.8\tilde{\sigma} - 6.8\pi\sqrt{2\tilde{\sigma}\tilde{\tau}} = 7.8R\sqrt{\frac{\sigma}{\kappa}} - 6.8\pi R\sqrt[4]{\frac{4\sigma\tau^2}{\kappa^3}} \quad (\tilde{\sigma} \gg 1), \tag{46}$$

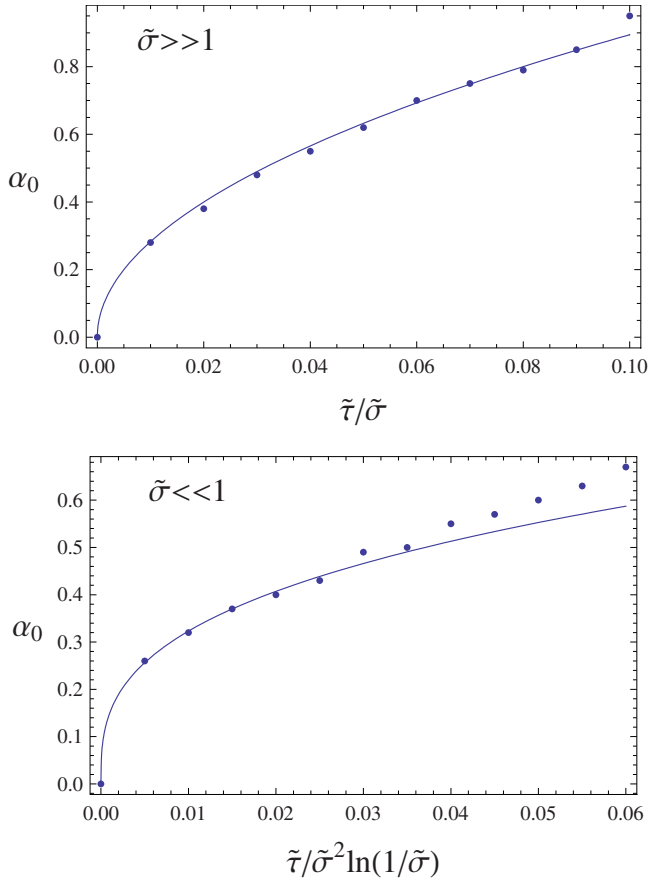

FIG. 7. (Color online) The capsid size α_0 as a free energy local minimum is shown as a function of $\tilde{\tau}/\tilde{\sigma}$ and $\tilde{\tau}/\tilde{\sigma}^2\ln(1/\tilde{\sigma})$ at two limits of $\tilde{\sigma}$. The dots are numerical results taken at $\tilde{\sigma}=10^2,10^3,10^4,10^5$ for the upper panel and $\tilde{\sigma}=10^{-2},10^{-3},10^{-4},10^{-5}$ for the lower panel. The curves are analytical results of Eq. (40) at $\tilde{\sigma}\gg 1$ and Eq. (37) at $\tilde{\sigma}\ll 1$ with additional numerical factors of 2 and 1.5, respectively. The range of $\tilde{\tau}$ plotted corresponds to the lower-right-hand "phase" in the "phase diagram" of Fig. 6.

$$\tilde{f}_m-\tilde{f}_0 \simeq 4.4\tilde{\sigma}^2\ln(1/\tilde{\sigma}) - 12.8\pi\sqrt[3]{\tilde{\tau}^2\tilde{\sigma}^2\ln(1/\tilde{\sigma})}$$
$$= 4.4R^2\frac{\sigma}{\kappa}\ln\frac{\sqrt{\kappa/\sigma}}{R} - 12.8\pi\frac{R}{\kappa}\sqrt[3]{\tau^2\sigma\ln\frac{\sqrt{\kappa/\sigma}}{R}} \quad (\tilde{\sigma} \ll 1). \tag{47}$$

The largest barriers are achieved at $\tilde{\tau}=0$ or $\tilde{f}_0=0$.

VI. KINETICS OF HIV BUDDING AND PARTIAL BUDDING

As discussed in the preceding sections, with a finite Gag-Gag attraction, budding always proceeds to completion thermodynamically. However, when this attraction is weak, or τ is small, a metastable state of partial budding appears at a smaller capsid size α_0 (see Fig. 3). It is therefore possible that the budding process is kinetically trapped at α_0. In this section, we discuss this kinetic effect and make connections of our theory to experiments.

Let us first estimate the values of parameters. A normal plasma membrane has $\kappa\simeq 20-40k_BT$ and $\sigma \simeq 0.5-2$ pN/nm$=0.12-0.48k_BT$/nm^2 [31]. On the other hand, typical HIV have $R\simeq 60-80$ nm [1]. Consequently, $\tilde{\sigma}=R\sqrt{\sigma/\kappa}\simeq 10$ and only the stiff membrane regime with $\tilde{\sigma}\gg 1$ is relevant for HIV. In this section, we therefore focus on the stiff membrane regime only. [In the opposite regime of $\tilde{\sigma}\ll 1$, the elastic energy scale is given by $\varepsilon_m\sim\kappa\tilde{\sigma}^2\ln(1/\tilde{\sigma})$, which may be comparable with k_BT and become unimportant.]

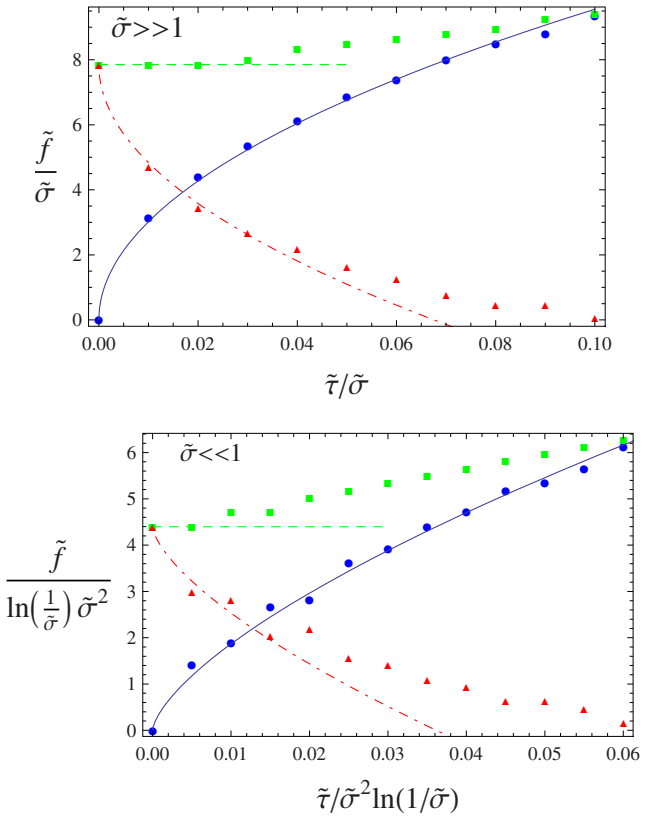

FIG. 8. (Color online). The local minimum $\tilde{f}_0$, maximum $\tilde{f}_m$, and barrier $\tilde{f}_m-\tilde{f}_0$ of the free energy density. The values of $\tilde{\sigma}$ and $\tilde{\tau}$ plotted are the same as in Fig. 7. The circles (blue) are the numerical result of $\tilde{f}_0$, fitted by the solid lines (blue) using Eq. (41) at $\sigma \gg 1$ and Eq. (38) at $\sigma\ll 1$ with additional numerical factor 1.7 and 3.2, respectively. The squares (green) are the numerical result of $\tilde{f}_m$, marked by the dashed lines (green) at their zero $\tilde{\tau}$ values. The triangles (red) are numerical result of the barriers, $\tilde{f}_m-\tilde{f}_0$, fitted by the dotted-dashed lines (red) using Eqs. (46) and (47).

In order to see if budding can be kinetically trapped at the local minimum α_0 (see Fig. 3), we must study the budding kinetics and calculate the kinetic barrier. For this purpose, let us employ the standard kinetic picture of the first-order phase transition [32,33], corresponding to the transition from a free-Gags phase to an aggregated Gags phase where Gags self-assemble into complete viral capsids. At the initial stage of aggregation, the concentration of free Gags is large, Gags coagulate to form dimers. Dimers coagulate with free Gags or other dimers to form larger Gag clusters (small capsids). This initial coagulation or nucleation is a fast process and is not a rate limiting step in retroviral budding. Soon free Gags are significantly depleted, and the main kinetic pathway for growth of capsids is for them to diffuse and merge with each

other. We will be concerned with this later stage of coagulation. For simplicity, we work with the dominant capsid size, $\alpha(t)$ [with concentration $n(t)$], assuming these typical capsids carry all the mass of membrane-bound Gag proteins.

Let us start with the case when $\alpha(t)$ is still small so that the energy barrier for merging of capsids is smaller than k_BT. This is the regime of the well-known diffusion-limited aggregation [34]. The rate of the capsid area $A(\alpha,t)$ incretion is proportional to the probability that two capsids diffuse and merge with each other. The kinetic rate equation reads as

$$\frac{dA(\alpha,t)}{dt} = 2\pi R \sin\alpha(t) A(\alpha,t) D \nabla n(t)|_{R\sin\alpha}, \quad (48)$$

where $D \simeq k_BT \ln[L/R\sin\alpha(t)]/\eta b$ is the lateral diffusion constant of a capsid on the membrane [35], L and b are the size and the thickness of the membrane. The $\nabla n(t)|_{R\sin\alpha}$ is the gradient of the concentration $n(t)$ on the edge of the capsid. This gradient can be estimated assuming a steady state in the diffusion and taking the adsorbing boundary condition at the edge of the capsid and a given capsid concentration [Eq. (3)] far away from the capsid. Solving the diffusion equation with these boundary conditions, we find

$$\nabla n(t)|_{R\sin\alpha} = \frac{c_G A(\alpha_G)}{A(\alpha) R \sin\alpha \ln(L/R\sin\alpha)}. \quad (49)$$

Substituting these relations and Eq. (4) into Eq. (48), we obtain

$$\cos\alpha(t) = \cos\alpha_G - \frac{t}{\tau_{\rm diff}}, \quad (50)$$

where

$$\tau_{\rm diff} = R^2 \eta b / k_B T c_G A(\alpha_G) \quad (51)$$

is the time scale of diffusion proportional to the viscosity η of the membrane. In the small α regime corresponding to a small kinetic barrier, this equation can be written as

$$\alpha(t) = (2t/\tau_{\rm diff} + \alpha_G^2)^{1/2}, \quad (52)$$

which is a slow function of time.

The regime of diffusion-limited growth stops when the kinetic barrier between approaching partial capsid is much larger than k_BT. At a later time, a different growth regime of Lifshitz-Slezov (LS) comes into play [32]. In this mechanism, the growth is no longer due to collision and merging of partially budded capsids. Instead, smaller capsids shrink and release individual Gags. These Gags are absorbed into larger capsids, leading to their growth. This process of releasing and adsorbing of individual Gags (the so-called coalescence) has much smaller kinetic barrier than the barrier to capsid merging in this later stage. The growth of capsid size in the LS regime is the same as that of diffusion-limited growth [32]. However, the rate constant $\tau_{\rm LS}$ depends exponentially on the activation energy to release individual Gag proteins from a capsid

$$\tau_{\rm LS} \propto \exp(-|\epsilon|/k_BT), \quad (53)$$

where ϵ is the binding energy of the Gag in a capsid, which itself is also a function of the Gag-Gag interaction.

The kinetic picture described above is good when $\tau > \tau_c$ and the free energy density decreases monotonically with increasing α (the left-hand panel of Fig. 3). However, when $\tau < \tau_c$ and a local minimum α_0 appears in the free energy density (the right-hand panel of Fig. 3), the above picture must be modified. For the cluster growth, either in the diffusion-limited regime or in the LS regime, the growth of the cluster size always reduces the free energy of the system. On the other hand, for the capsid growth of retroviral budding, after the capsid size reaches α_0, the system free energy increases when the capsids grow further. For $\alpha > \alpha_0$, the growth of capsids is determined by the ability to overcome the kinetic barrier related to $f_m - f_0$ (see Fig. 3). The detailed analysis of the rate of capsid growth for $\alpha > \alpha_0$ is a very interesting problem by itself, requiring understanding of membrane energetics when a partially budded capsid absorbs other capsids or many individual Gags to increase its size from α_0 to α_m. These calculations are beyond the scope of this paper and we will leave the detail treament of capsid growth in this case to a future study. Nevertheless, one can expect the rate of such process to be inversely proportional to the exponential of the energy barrier

$$\tau_m \propto \exp[-(f_m - f_0)/nk_BT], \quad (54)$$

where $(f_m - f_0)/n$ is the energy barrier of a membrane cell with a single capsid in it. According to Eqs. (46) (see also the upper panel of Fig. 8), the maximum energy barrier is achieved at $f_0 = 0$ or $\tilde{\tau} = 0$. Using Eqs. (3) and (34), it can be written as

$$E_m = \frac{f_m}{n} = \kappa(1 - \cos\alpha_m)\tilde{f}_m, \quad (55)$$

where $\tilde{f}_m$ is given by Eqs. (46), and α_m is the corresponding capsid size. A more useful expression of E_m can be obtained if one recognizes that E_m is nothing but the maximum of ε_m shown in Fig. 5. Using the numerical result of that figure, we obtain

$$E_m = 11.5\kappa\tilde{\sigma} = 11.5R\sqrt{\kappa\sigma}. \quad (56)$$

Clearly, $E_m \gg k_BT$ for $\tilde{\sigma} > 1$. For example, for $R = 70$ nm, $\sigma = 0.24 k_BT/\text{nm}^2$ and $\kappa = 20 k_BT$, we obtain $E_m = 1765 k_BT$. The true energy barrier is smaller than E_m since $\tilde{\tau} > 0$. In the regime of small $\tilde{\tau}$, according to Eq. (46), it is

$$E \simeq \kappa(1 - \cos\alpha_m)(\tilde{f}_m - \tilde{f}_0) = E_m\left(1 - 3.9\sqrt{\frac{\tilde{\tau}}{\tilde{\sigma}}}\right)$$
$$= E_m\left(1 - 3.9\sqrt[4]{\frac{\tau^2}{\kappa\sigma}}\right). \quad (57)$$

In experiments, for normal plasma membranes with given κ and σ, according to Eq. (56), the larger the retrovirus size R, the larger the kinetic barrier. On the other hand, the line tension τ is directly proportional to the strength of the Gag-Gag attraction and is experimentally adjustable through mutation of the late domain on the Gag protein, binding of other molecules to Gags or changing the pH, salinity of water solution near the membrane [2,15]. As we know, the closest approach distance between two Gag proteins is about 10 nm

[1]. Taking a rough estimate for the Gag-Gag pair interaction energy as $10k_BT$ (see Sec. V of Ref. [36] for details), and assuming Gags are densely packed on the capsid, one obtains $\tau \simeq 1k_BT/\mathrm{nm} \simeq 4$ pN for normal retroviral capsids. Theoretically, in order to have a local minimum in the free energy density and trap retrovirus budding kinetically, we must have $\tau < \tau_c$ (see Fig. 3). For a normal cell membrane with $\kappa = 20k_BT$ and $\sigma = 0.24k_BT/\mathrm{nm}^2$, using Eq. (44), $\tau_c \simeq 0.24k_BT/\mathrm{nm} = 1$ pN. Therefore, for normal capsids, $\tau > \tau_c$, and budding easily proceeds to completion (see the left-hand panel of Fig. 3). On the other hand, τ is larger than τ_c only by a factor of 4. Therefore, HIV budding can be fairly easily trapped at a partially budded state with capsid size α_0 by reducing the Gag-Gag interaction strength such as mutation of a single domain on the Gag protein. The kinetic barrier E that appeared at $\alpha = \alpha_0$ can be much larger than k_BT, and the time scale for capsid growth beyond α_0, τ_m, is exponentially large. Qualitatively, this trend is consistent with experiments on mutation of the late domain of Gag proteins [2,3]. Numerically, we know that $\alpha_0 < 0.9 \simeq 0.3\pi$ (see the upper panel of Fig. 7). It agrees with experiments reasonably well.

It is worth to point out that some practical factors in retrovirus budding and assembly have been neglected in our simple model, such as local variation in membrane elasticity due to raft structures which seem preferred by retroviruses budding [37], or the presence of other proteins in in-vivo assembly and budding [2]. Therefore one cannot expect our model to explain everything. On the other hand, more controlled experiments are needed to verify the dependence on the membrane rigidities and Gag-Gag attraction of α_0 given by Eq. (40).

VII. CONCLUSION

In this paper, we developed a model of HIV (and retroviruses in general) budding and self-assembly on the elastic membrane. We studied the free energy profile of the system as a function of the capsid size α. We showed that although always thermodynamically favorable, complete budding and assembly may not be achieved, due to the presence of a metastable state at the capsid size α_0 if the Gag-Gag attraction is weak. In practice, for normal biological conditions, the Gag-Gag attraction is strong enough and HIV budding and assembly always proceed to completion, as it should be. On the other hand, it is fairly easy to trap HIV budding to a partially budded state at α_0 by reducing the Gag-Gag attraction. This can be done through the mutation of late domain on the Gag protein or binding of other molecules to Gag, or by increasing the membrane rigidities, although this may not be easy to do in-vivo. Our theory agrees reasonably well with experimental results. However, experiments with better controlled environments are needed to verify various aspects of the theory.

The most interesting point of our model is probably that it provides a unique self-assembly mechanism. Not like self-assembly of other viruses or colloids, HIV assemble and bud *concurrently* on the membrane. Therefore, the membrane elastic energy plays an important role in the assembly process. For example, the kinetic barrier which traps the HIV budding essentially comes from the membrane elastic energy. In fact, our model developed for HIV budding and assembly can be very well applied to other situations. For example, for a given concentration of membrane-bounded proteins with a fixed spontaneous curvature, this kind of budding and assembly phenomenon should also exist and can be explained using our model. In this situation, it may be easier to change the membrane properties and protein-protein attraction in vitro to verify our theory more quantitatively. Due to the interplay between the membrane elastic energy and the Gag-Gag attraction energy, the kinetics of retrovirus budding is an interesting problem by itself, and will be addressed in more details in the near future. In this paper, we limit our consideration to the case of low Gag concentration, c_G, and assume that capsids do not interact. Future work will consider higher Gag concentration ($c_G > 0.1\ \mathrm{nm}^{-2}$) where capsid-capsid interaction can be important.

ACKNOWLEDGMENTS

We wish to thank G. Bel, J. Mueller, B. I. Shklovskii, and T. A. Witten for useful discussions. T.T.N. acknowledges the junior faculty support from the Georgia Institute of Technology.

[1] J. M. Coffin, S. H. Hughes, and H. E. Varmus, *Retroviruses*, 1st ed. (Cold Spring Harbor Laboratory Press, New York, 1997).
[2] E. Morita and W. I. Sundquist, Annu. Rev. Cell Dev. Biol. **20**, 395 (2004).
[3] D. G. Demirov and E. O. Freed, Virus Res. **106**, 87 (2004).
[4] E. Gottwein, S. Jäger, A. Habermann, and H.-G. Krässlich, J. Virol. **80**, 6267 (2006).
[5] S. Tzlil, M. Deserno, W. M. Gelbart, and A. Ben-Shaul, Biophys. J. **86**, 2037 (2004).
[6] M. Deserno and T. Bickel, Europhys. Lett. **62**, 767 (2003).
[7] M. Deserno, Phys. Rev. E **69**, 031903 (2004).
[8] A. Zlotnick, J. Mol. Biol. **366**, 14 (2007).
[9] M. F. Hagan and D. Chandler, Biophys. J. **91**, 42 (2006).
[10] T. Hu and B. I. Shklovskii, Phys. Rev. E **75**, 051901 (2007).
[11] S. D. Hicks and C. L. Henley, Phys. Rev. E **74**, 031912 (2006).
[12] J. E. Dooher, B. L. Schneider, J. C. Reed, and J. R. Lingappa, Traffic (Oxford, U. K.) **8**, 195 (2007).
[13] H. Garoff, R. Hewson, and D.-J. E. Opstelten, Microbiol. Mol. Biol. Rev. **62**, 1171 (1998).
[14] S. Welsch, B. Müller, and H. Kraüsslich, FEBS Lett. **581**, 2089 (2007).
[15] S. Campbell, R. J. Fisher, E. M. Towler, S. Fox, H. J. Issaq, T. Wolfe, L. R. Phillips, and A. Rein, Proc. Natl. Acad. Sci. U.S.A. **98**, 10875 (2001).

[16] F. Jülicher and R. Lipowsky, Phys. Rev. Lett. **70**, 2964 (1993).
[17] F. Jülicher and R. Lipowsky, Phys. Rev. E **53**, 2670 (1996).
[18] P. Canham, J. Theor. Biol. **26**, 61 (1970).
[19] W. Helfrich, Z. Naturforsch. C **28C**, 693 (1973).
[20] In Ref. [17], the Gaussian curvature term is important since the area of the budding region is not fixed.
[21] Kreyszig, *Differential Geometry* (Dover, New York, 1991).
[22] Expansion in the opposite limit $|\nabla h| \gg 1$ gives a nonlinear differential equation which cannot be solved analytically.
[23] L. D. Landau and E. M. Lifshitz, *Statistical Physics, Part 1*, 3rd ed. (Butterworth Heinemann, Oxford, 1980).
[24] In the opposite limit of $\kappa=0$, although $\delta\varepsilon_m=0$ still has a catenoid solution, it is only a stationary solution but does not correspond to an energy minimum. Actually ε_m can be arbitrarily close to zero but not equal to zero, given a membrane shape arbitrarily close to the flat membrane and only deformed a little bit at the capsid rim. This result is different from the minimal surface of revolution problem in the calculus of variation [25]. This is essentially due to the fact that our boundary condition requires the membrane to be flat at infinity, but there is no confinement to its position there.
[25] B. van Brunt, *The Calculus of Variations* (Springer, New York, 2004).
[26] Since all energies we considered are positive definite, $H=0$ corresponds to an absolute minimum for ε_m. One can of course still use $\delta\varepsilon_m=0$ to obtain an elastic equation. It is much more complicated than $H=0$ and the catenoid solution indeed holds.
[27] F. Morgan, *Riemannian Geometry: A Beginner's Guide*, 1st ed. (Jones and Bartlett, Boston, London, 1993).
[28] The first-order correction to this solution for large but finite r_s also involves a nonlinear differential equation and cannot be solved analytically.
[29] U. Seifert, K. Berndl, and R. Lipowsky, Phys. Rev. A **44**, 1182 (1991).
[30] Intuitively, one may think that at α close to π, the "neck" of the membrane (see the lower-right-hand panel of Fig. 4 for an illustration of the neck) cost a large elastic energy. In fact, this is not the case. In the soft membrane regime, the bending energy dominates. This neck can take a catenoid shape which has zero curvature energy. In the stiff membrane regime, the stretching energy dominates. The membrane can make a sharp turn to minimize the stretching energy again to almost zero.
[31] C. E. Morris and U. Homann, J. Membr. Biol. **179**, 79 (2001).
[32] E. M. Lifshitz and L. P. Pitaevskii, *Physical Kinetics* (Butterworth-Heinemann, Oxford, 1997).
[33] T. T. Nguyen and B. I. Shklovskii, Phys. Rev. E **65**, 031409 (2002).
[34] D. F. Evans and H. Wennerström, *The Colloidal Domain: Where Physics, Chemistry, Biology, and Technology Meet*, 2nd ed. (Wiley-VCH, New York, 1999).
[35] P. G. Saffman and M. Delbrück, Proc. Natl. Acad. Sci. U.S.A. **72**, 3111 (1975).
[36] T. T. Nguyen, R. F. Bruinsma, and W. M. Gelbart, Phys. Rev. E **72**, 051923 (2005).
[37] N. Chazal and D. Gerlier, Microbiol. Mol. Biol. Rev. **67**, 226 (2003).